

# The stability margin for stable weightless liquid bridges<sup>a)</sup>

Lev A. Slobozhanin,<sup>b)</sup> J. Iwan D. Alexander, and Viral D. Patel

*Department of Mechanical and Aerospace Engineering and National Center for Microgravity Research on Fluids and Combustion, Case Western Reserve University, Cleveland, Ohio 44106*

(Received 6 February 2001; accepted 3 October 2001)

The stability of weightless axisymmetric liquid bridge equilibrium configurations to “large” disturbances is examined by calculating the stability margin. For bridges held between coaxial equidimensional circular disks (radius  $R_0$ ) separated by a distance  $H$ , the stability to infinitesimal perturbations (linear stability) has been thoroughly investigated and the stability region is constructed in the  $(\Lambda, V)$  plane. Here, the slenderness  $\Lambda$  ( $=H/2R_0$ ) and the relative volume  $V$  (ratio of the actual liquid volume to that of a cylinder with radius  $R_0$  and height  $H$ ) are the parameters that define the system. To assess stability with respect to finite amplitude disturbances we use a potential energy analysis based on the concepts of a potential energy well and the equilibrium stability margin introduced by Myshkis [USSR Comput. Math. Math. Phys. **5**, 193 (1965); Math. Notes Acad. Sci. USSR **33**, 131 (1983); *Introduction to the Dynamics of a Body Containing a Liquid Under Zero-Gravity Conditions* (Vychisl. Tsentr Akad. Nauk SSSR, Moscow, 1968)]. The stability margin represents the height of a local potential energy barrier adjacent to the well of a given stable equilibrium. Wherever a linearly stable equilibrium is nonunique equilibrium, the stability margin corresponds to the smallest among the heights of saddle points on the potential energy surface that are adjacent to the well. The saddle point that determines the stability margin is the point of emergence from the well and leads to the energy wells corresponding to other equilibria or to infinity. Unless the total energy of perturbations exceeds the stability margin for a given stable equilibrium, the liquid bridge will return to that equilibrium state. In this work we determined the stability margin in part of the stability region where axisymmetric bridges that are already unstable to small axisymmetric perturbations coexist with stable ones. The domains of existence of a variety of unstable axisymmetric bridges are constructed using previous results concerning the bifurcation structure. This enabled us to construct contours of the dimensionless stability margin within the linear stability region not only in the vicinity of the stability boundary, but also far from it. The stability margins for bridges with fixed values of the slenderness, as well as for cylindrical and catenoidal bridges, are also calculated. © 2002 American Institute of Physics.  
[DOI: 10.1063/1.1420736]

## I. INTRODUCTION

### A. Stability margin

The stability margin can be considered as the upper limit of the values of kinetic energy that can be attained by a system and still return to the equilibrium state in the case of the slightest dissipation of energy. For a stable equilibrium state of an autonomous potential *mechanical system*, the stability margin,  $\mathcal{M}$ , represents the height of a local potential barrier (or the depth of a potential well) and can also be defined as

$$\mathcal{M} = (U_e - U_s), \quad (1)$$

where  $U_e$  is the value of the potential energy at the point of emergence from the potential well, and  $U_s$  is the value of the potential energy at the bottom of the well, i.e., at the stable equilibrium state under consideration. For mechanical sys-

tems with a finite number of degrees of freedom, the point of emergence represents a saddle point of the potential energy function  $U$ . A method of calculating the stability margin based on trapping the location of this point was proposed by Myshkis.<sup>1</sup>

Myshkis<sup>1</sup> examined the concept of a well and its properties (the most important of which is the depth of the well) for analytic functions in  $n$ -dimensional space. He then extended these considerations to arbitrary lower semi-continuous functions in an arbitrary topological space.<sup>2</sup> This mathematical theory has an immediate physical interpretation in the case when the function is the potential energy of a system.

Myshkis<sup>3</sup> also pioneered the application of the important concept of the stability margin for stable equilibrium states of a *capillary liquid*. The formal definition of the stability margin in problems of fluid mechanics causes considerable difficulties that have not yet been overcome. These difficulties have the same origin as those noted by Lyapunov in defining the very concept of the equilibrium stability of a

<sup>a)</sup>Dedicated to Professor A. D. Myshkis on the occasion of his 80th birthday.

<sup>b)</sup>Center for Microgravity and Materials Research, University of Alabama in Huntsville, Huntsville, AL 35899.

liquid. The reason is that infinitely thin filament-type protrusions (in the case of capillary liquid) or sheet-type protrusions (if capillary forces are not taken into account) on the surface of the liquid system can change the surface configuration but do not change the system's potential energy. The possibility of removing small droplets under specially distributed small perturbations such as these must not contradict the existence of a total stability margin, a transition through which leads to a considerable change in the equilibrium state. The possible ways of dealing with these difficulties were also first discussed by Myshkis.<sup>3</sup> Later Myshkis and his co-workers developed these approaches and used them for solution of specific problems. These works were published in Russian and later summarized in English in Ref. 4.

One approach is based on an extension of formula Eq. (1) to a capillary liquid when an unstable equilibrium state determining  $U_e$  can be detected. This approach is the most effective but requires study of the bifurcation of equilibrium states at the stability region boundary. If the bifurcation is subcritical, i.e., it takes place toward the stability region, then, for the same values of the parameters belonging to this region, there are two equilibrium states close to the critical one: an unstable state that bifurcates from the critical state, and the stable one. In analogy with Eq. (1), the stability margin of the stable equilibrium is determined by measuring the difference between the potential energy levels of the unstable state and of the stable state under consideration.

There are several equilibrium systems with a capillary liquid for which the stability margin was estimated using this approach. They include a liquid suspended in a circular cylindrical container, an axisymmetric pendant drop on a horizontal plane, and related plane equilibrium problems (see Ref. 4, pp. 240–242, 245–246, 257–262). The stability margin for a soap film spanning two open equal-diameter end-rings was examined theoretically and experimentally by Cryer and Steen.<sup>5</sup> However, there is no systematic solution of the stability margin problem for liquid bridges. The goal of this paper is the estimation of the stability margin for stable axisymmetric states of a weightless liquid bridge. The bridge has a free surface pinned to edges of two coaxial equidimensional circular disks. Perturbations of this free surface satisfy the constraints of constant liquid volume and fixed contact lines. Such a liquid bridge system is interesting not only in itself, but also because an understanding of weightless bridges provides us with a basis for the interpretation of the behavior of bridges subject to a potential force field or constrained by supports with more complicated geometries. Because of their occurrence in a variety of technological and physical systems, liquid bridges have been the subject of investigation for more than a century beginning with the celebrated work of Plateau.<sup>6</sup> There are numerous publications on equilibrium and linear stability problems for this system (see, for example, Myshkis *et al.*,<sup>4</sup> Gillette and Dyson,<sup>7</sup> Michael,<sup>8</sup> Boucher and Jones,<sup>9</sup> Lowry and Steen,<sup>10</sup> Slobozhanin *et al.*,<sup>11</sup> and references therein).

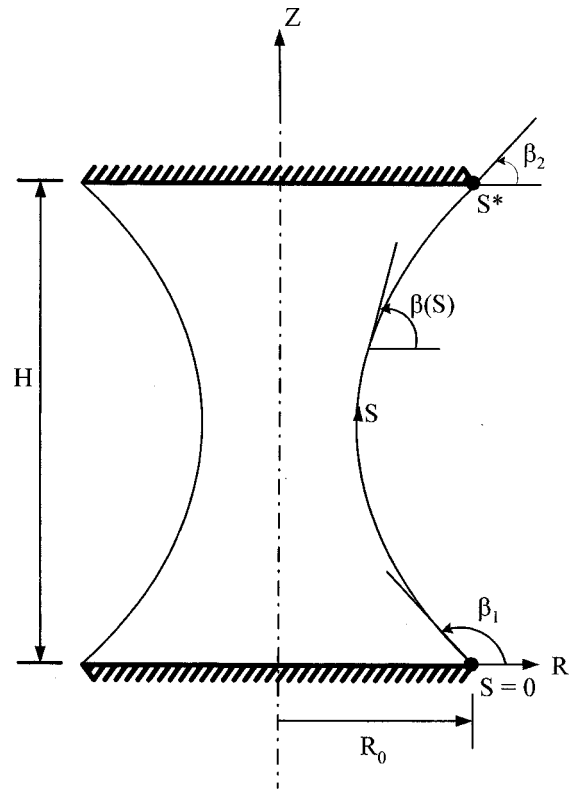


FIG. 1. Geometry and coordinate system for the equilibrium liquid bridge problem.

## B. Linear stability and bifurcation of the equilibrium states of a weightless axisymmetric liquid bridge

In this section, we summarize previous results that are relevant to the liquid bridge stability margin problem and outline the approach used in this paper.

The equilibrium surface of an axisymmetric liquid bridge has a parametric representation  $R(S)$ ,  $Z(S)$ , where  $R$ ,  $\Theta$  and  $Z$  are the cylindrical coordinates, and  $S$  is the arc length of an axial section,  $\Theta = \text{const}$ , of the surface (Fig. 1). The equilibrium and stability of such a liquid bridge are determined by two parameters: the slenderness (or the aspect ratio),  $\Lambda$ , and the relative volume,  $V$ . They are defined as

$$\Lambda = H/(2R_0), \quad V = \nu/(\pi R_0^2 H). \quad (2)$$

Here  $R_0$  is the disk radius,  $H$  is the disk separation, and  $\nu$  is the actual liquid volume (Fig. 1). Three parameters are necessary to characterize the shape of an axisymmetric liquid bridge and to determine the values of  $\Lambda$  and  $V$ . These parameters are either of the slope angles,  $\beta_1$  or  $\beta_2$ , of the surface profile at the end-points of the profile (Fig. 1), the mean curvature of the surface, and the number,  $k$ , of extreme points possessed by  $R(S)$  between the profile's endpoints (i.e., the endpoints are not counted). With the exception of a cylindrical bridge, an axisymmetric bridge may be stable<sup>7</sup> only if its surface profile has just one inner extreme point of  $R$ , i.e., when  $k=1$ . Such a bridge necessarily has an equatorial symmetry plane  $Z=H/2$ . The same is true for a critical, i.e., neutrally stable, bridge.

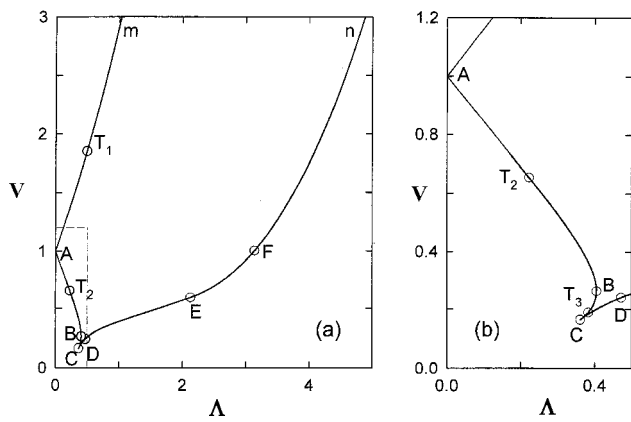


FIG. 2. Stability diagram for axisymmetric weightless liquid bridges: (a) general view; (b) inset related to the ABC segment (from Ref. 11).

The boundary of the stability region (Fig. 2) consists of two nonintersecting branches. Along the upper branch  $Am$ , the surfaces of critical bridges are rotund nodoids with convex profiles and horizontal tangents at the endpoints of the profiles ( $\beta_1=0$  and  $\beta_2=180^\circ$ ). Here loss of stability occurs with respect to nonaxisymmetric perturbations. The component  $\mathcal{N}$  of critical perturbations normal to the axisymmetric equilibrium surface is proportional to  $Z'(S)\sin\Theta$ . Along the right-hand branch  $CDEFn$  of the lower boundary (Fig. 2), stability is lost to axisymmetric perturbations. Surfaces of critical bridges corresponding to points along  $EFn$  are rotund (within  $Fn$ ) or constricted (within  $EF$ ) unduloids with profiles that have vertical tangents at the endpoints ( $\beta_1=\beta_2=90^\circ$ ). At the point  $F$  ( $V=1, \Lambda=\pi$ ), the critical surface is a cylinder. For critical bridges along  $EFn$ , the component  $\mathcal{N}$  is proportional to  $R'(S)$  for critical unduloids and to  $\sin[\pi(2Z-H)/H]$  for the critical cylinder. Thus, the critical perturbations are reflectively antisymmetric about the equatorial plane.

For bridges corresponding to inner points of the segment  $CDE$ , the critical surfaces are constricted unduloids within the segment  $DE$ , a catenoid at the point  $D$ , and constricted nodoids within  $CD$ . These surfaces have profiles with  $90^\circ < \beta_1 < 180^\circ$ . Here, critical axisymmetric perturbations are reflectively symmetric about the equatorial plane, in contrast to those along  $EFn$ . Finally, the left-hand segment  $ABC$  of the lower boundary corresponds to constricted nodoids that have concave profiles with horizontal tangents at the endpoints ( $\beta_1=180^\circ$  and  $\beta_2=0$ ). These so-called limiting surfaces are also the ones that are critical with respect to non-axisymmetric perturbations with  $\mathcal{N}$  proportional to  $Z'(S)\sin\Theta$ .

The shape of a critical perturbation defines (to a first approximation in the vicinity of the critical state) the shape of a bridge surface that bifurcates from the critical state. Liquid bridge surfaces that bifurcate from critical states corresponding to points of  $CDEFn$  are axisymmetric. For the boundary segment  $mABC$ , the bifurcating surfaces are non-axisymmetric. The bifurcation structure is of particular importance for the stability margin problem. It was found in Ref. 11 that the bifurcation is subcritical along the boundary segments  $T_1AT_2$  and  $T_3CDEFn$ , and is supercritical (i.e.,

out from the stability region) along the segments  $T_1m$  and  $T_2BT_3$  (see Fig. 2).

Aside from the nature of the critical perturbations, the shape of bifurcating surfaces depends on  $\Lambda$  and on the deviation  $\epsilon^2=|V-V^*|$  of the relative volume  $V$  from its critical value  $V^*(\Lambda)$ . To a first approximation in  $\epsilon$ , the shape of bifurcating bridges has been determined.<sup>11</sup> As a result, for given  $\Lambda$  and  $V$  in the stability region, we can find the shape of the stable axisymmetric bridge and the shape of the bifurcating bridge provided that the bifurcation is subcritical and  $\epsilon$  is small. Then we can obtain expressions for the stability margin of stable states located in the vicinity of the stability boundary segments  $T_1AT_2$  and  $T_3CDEFn$ . However, such results have limited applications because only a small region in the vicinity of the stability boundaries is considered. Furthermore, experiments<sup>11</sup> showed that the subcritical region adjacent to the segment  $T_1A$  (consisting of unstable nonaxisymmetric bridges) is a very thin layer. In addition, the boundary segments  $T_1AT_2$  and  $T_3C$  are small and are associated with short bridges ( $\Lambda < 0.495$ ).

Because of the above limitations associated with the stability margin for the boundary segment  $T_1AT_2$  and  $T_3C$ , we choose only to analyze the stability margin for the boundary segment  $CDEFn$ . However, our analysis is extended to points in the stability region that are far from this boundary. This can be accomplished by considering stable and unstable axisymmetric bridges associated with points in the stability region. Then we can directly apply the methods used to calculate axisymmetric equilibrium bridges, including unstable ones, and calculate the exact value of the potential barrier, not only in the vicinity of the boundary segment  $CDEFn$ , but also in a large part of the stability region. (We imply here, and show later in this paper, that there are no nonaxisymmetric bridges branching from unstable axisymmetric ones.)

It should be recalled that the stability region represents the region of stability with respect to infinitesimal perturbations of the free surface configuration. It is emphasized that if we know the height of a potential barrier inside the stability region and well away from the stability boundary, it is possible to estimate the degree of the equilibrium stability to perturbations of a finite magnitude.

For a zero-gravity liquid bridge system, the potential energy, to within a constant term, is determined by the free surface energy which is proportional to the free surface area. Haynes<sup>12</sup> has, for  $V=1$ , constructed the ratios of free surface areas of unduloidal and cylindrical configurations as a function of  $\Lambda$ . These ratios can be used to estimate the stability margin for stable cylindrical bridges. Boucher and Jones,<sup>9</sup> and Lowry and Steen<sup>10</sup> carried out a more sophisticated treatment of axisymmetric bridges that are unstable to axisymmetric perturbations. It must be emphasized that the results of the above works are necessary for the construction of the regions of existence of different unstable axisymmetric bridges and for understanding the nature of bifurcations among axisymmetric states. Boucher and Jones<sup>9</sup> have constructed the relationship between dimensionless free surface area,  $\Omega = \Gamma/R_0^2$  ( $\Gamma$  is the actual area), and dimensionless volume,  $\nu/R_0^3$ , for stable and unstable bridges at values of

$\Lambda=0.5, 1.0,$  and  $3.0$ . These  $\Lambda$  values are representative of the three types of bifurcation behavior. In terms of the wave number  $k$  (the number of inner extrema on the bridge profile), only unstable bridges with  $k=1, 2,$  and  $3$  (1 minimum and 2 maxima) are considered. Lowry and Steen<sup>10</sup> carried out a careful study of the bifurcation problem for axisymmetric bridges and constructed diagrams of equilibrium states. These diagrams relate  $V$  to  $\cos \beta_1$  and to the dimensionless pressure jump across the free surface for stable and all possible unstable bridges (this also includes bridges with  $k \geq 3$ ) at values of  $\Lambda=0.5, 1.0, \pi/2, 1.75, 2.0, 2.5,$  and  $\pi$ . However, there was no analysis of the free surface areas. The classification of axisymmetric capillary surfaces in terms of the wave number  $k$ , introduced by Lowry and Steen,<sup>10</sup> is very useful, especially for examination of unstable surfaces.

A simple mathematical approach outlined in Sec. II can be used to construct a family of axisymmetric bridges with fixed values of  $k$  and  $\beta_1$ . The shape of each bridge is calculated together with  $\Lambda, V$  and the dimensionless free surface area  $\Omega$ . Thus for fixed  $k$ , the line corresponding to a given  $\beta_1$  ("the level line  $\beta_1 = \text{const}$ ") can be constructed in the plane  $(\Lambda, V)$ . A set of the level lines related to different  $\beta_1$  offers a clearer view of the existence and nature of axisymmetric bridges with a given  $k$  in the  $(\Lambda, V)$  plane.

A dense family of the level lines for bridges with  $k=1$  is constructed in Sec. III. Such a bridge is either a stable bridge or an unstable one that determines the point of emergence from the potential well. Bridges with  $k=2$  (Sec. III) are equally important since they also determine the points of emergence from the potential wells. Bridges with  $k \geq 3$  (Sec. IV) are unrelated to the stability margin problem. Therefore, we do not consider the  $k \geq 3$  level lines in detail, but simply identify those parts of the stability region where bridges with  $k \geq 3$  exist and give examples of such bridges. In order to show that only unstable axisymmetric bridges with  $k=1$  and  $k=2$  serve as points of emergence we have verified that no nonaxisymmetric bridges bifurcate from these unstable axisymmetric bridges (Sec. V). A quite dense family of the level lines can be used to construct the surface  $\Omega(\Lambda, V)$  for  $k=1$  and  $k=2$ . This is most important because the stability margin for a zero-gravity liquid bridge system is determined by the difference in the dimensionless free surface area,  $\Omega$ , between unstable (with  $k=1$  or  $k=2$ ) and stable ( $k=1$ ) bridges. Comprehensive data required for calculation of the stability margin over a wide range of the parameters  $\Lambda$  and  $V$  are presented in Sec. VI.

## II. BRANCHES OF AXISYMMETRIC BRIDGES WITH A GIVEN WAVE NUMBER

In the following we employ dimensionless variables

$$r=R/R_0, \quad z=Z/R_0, \quad s=S/R_0, \quad (3)$$

where the disk radius,  $R_0$ , is the characteristic length. The functions  $r(s)$  and  $z(s)$  are the solutions of the following initial-value problem:<sup>4</sup>

$$r'' = -z' \beta', \quad z'' = r' \beta', \quad \beta' = q - z'/r, \quad \left( ' = \frac{d}{ds} \right) \quad (4)$$

$$\begin{aligned} r(0) &= 1, \quad r'(0) = \cos \beta_1, \quad z(0) = 0, \\ z'(0) &= \sin \beta_1, \quad \beta(0) = \beta_1. \end{aligned} \quad (5)$$

Here,  $q$  is twice the mean curvature of the surface, and  $\beta = \beta(s)$  is the angle between the positive  $r$ -axis and the tangent to the axial profile in the direction of increasing  $s$  (see Fig. 1).

In addition to  $\beta_1$  and  $q$ , the shape of an axisymmetric surface is characterized by the wave number  $k$ . For our purposes it will suffice to consider values of  $\beta_1$  from the interval  $0 \leq \beta_1 \leq 180^\circ$ . To find the characteristics of bridges with given  $\beta_1$  and  $k$ , we choose some value  $q = q_0$  and numerically integrate the system Eq. (4) with the initial conditions Eq. (5) using a sixth-order Runge–Kutta technique with variable step size. For  $\beta_1 \neq 90^\circ$ , the integration process continues until the point  $s = s^*$  where the function  $r(s)$  becomes equal to 1 for the  $k$ th time (not counting the point  $s=0$ ). If  $\beta_1 = 90^\circ$ , only bridges with odd  $k$  are possible. In this case, the point  $s = s^*$  corresponds to the point at which the function  $r(s)$  becomes equal to 1 for the  $(k+1)/2$ -th time (not counting the point  $s=0$ ). The curve  $r(s), z(s) (0 \leq s \leq s^*)$  that is constructed in this manner represents the equilibrium surface profile only if it is not self-intersecting. Self-intersection occurs when the equilibrium profile has a so-called double point<sup>13</sup> where the same value  $(r, z)$  occurs for two different values of  $s$ . Whether or not the profile is self-intersecting depends on the value of  $q$  for a given  $\beta_1$  and  $k$ . Only nodoidal-type integral curves may be self-intersecting.

The following quantities are to be calculated during the integration process along the equilibrium profile:

$$\begin{aligned} h &= z(s^*), \quad \Lambda = h/2, \quad V = \frac{1}{h} \int_0^{s^*} r^2(s) z'(s) ds, \\ \Omega &= 2\pi \int_0^{s^*} r(s) ds. \end{aligned} \quad (6)$$

The above values of  $\Lambda$  and  $V$  determine a point in the  $(\Lambda, V)$  plane that corresponds to a bridge with given  $\beta_1$  and  $k$ . The quantity  $\Omega$  represents the dimensionless area of the bridge's free surface. Since the "disk-gas" and "disk-liquid" interfacial energies are the same for different bridge configurations, they may be ignored in calculation of the stability margin. Thus it is assumed that the potential energy of a bridge is equal to the energy of its free surface. Then

$$\Omega = \frac{U}{\sigma R_0^2}, \quad \Sigma = \Omega_e - \Omega_s = \frac{\mathcal{M}}{\sigma R_0^2}, \quad (7)$$

where  $\sigma$  is the surface tension,  $U$  is the potential energy of an axisymmetric bridge, and  $\Sigma$  is the dimensionless stability margin.

By choosing closely spaced values of  $q$ , we can obtain a dense sequence of points in the  $(\Lambda, V)$  plane. The locus of these points is a curve that represents the level line  $\beta_1 = \text{const}$  for a given  $k$ . The value of  $\Omega$  can also be calculated along this curve. Obviously, the construction of such a curve only has meaning inside the stability region shown in Fig. 2. Each set of level lines for stable and unstable bridges with

TABLE I. Properties of characteristic points.

Point	$\Lambda$	$V$	Stable ( $k=1$ )			Unstable ( $k=1$ or $2$ )			$\Sigma$
			$\beta_1$ [deg]	$q$	$\Omega$	$\beta_1$ [deg]	$q$	$\Omega$	
C	0.361	0.164	180	-0.449	6.54	180	-0.449	6.54	0
D	0.4718	0.2405	167.84	0	6.77	167.84	0	6.77	0
E	2.129	0.591	90	1.412	20.66	90	1.412	20.66	0
F	$\pi$	1	90	1	$4\pi^2$	90	1	$4\pi^2$	0
G	0.308	0.516	180	-2.147	5.15	145.81	1.124	6.88	1.73
I	1	2/3	116.64	0.732	10.77	90	2	$4\pi$	1.80
J	1.788	1.033	88.79	0.996	22.85	51.80	1.372	25.01	2.16
K	3.436	1.210	90	0.912	47.51	90	0.912	47.51	0
L	2	2/3	97.56	1.175	20.67	71.6	1.431	20.92	0.25
M	2.930	0.876	90	1.071	34.46	90	1.071	34.46	0
N	2.243	0.615	90	1.355	22.18	90	1.355	22.18	0
O	1.811	0.662	100.3	1.140	18.72	69.67	1.516	19.19	0.47
P	3.066	1.033	89.89	0.984	39.17	76.70	1.010	39.19	0.02
Q	0	0.5	...	...	...	180	0	$2\pi$	...
T	$\sqrt{3/2}$	1	90	1	$4\sqrt{3/2}\pi$	54.74	1.633	$6\pi$	3.46
W	0.654	0.571	141.09	0.0	7.47	113.66	1.832	8.97	1.50
Y	2.139	0.593	90	1.406	20.80	90	1.406	20.80	0

given wavenumbers is associated with a set of characteristic points. Properties of these and other important points are summarized in Table I.

III. BRIDGES WITH THE WAVE NUMBERS  $k=1$  AND  $k=2$

Here we consider axisymmetric bridges with  $k=1$  and  $k=2$  since they are the most important for the stability margin problem.

A. Bridges with  $k=1$

For a stable noncylindrical bridge,  $r(s)$  has one inner extreme point. This point is a maximum for rotund bridges ( $V > 1$ ) and is a minimum when the bridge surface is constricted ( $V < 1$ ). Thus, for stable bridges with  $V \neq 1$ , we have  $k=1$ . However, as we will see later, bridges with  $k=1$  are not necessarily stable.

The behavior of level lines  $\beta_1 = \text{const}$  for  $k=1$  is quite simple when  $V > 1$  (see Fig. 3). The lines  $\beta_1 = \text{const}$  with  $0 < \beta_1 < 90^\circ$  correspond to stable surfaces, while the lines  $\beta_1 = 0$  (branch  $Am$ ) and  $\beta_1 = 90^\circ$  (branch  $Fn$ ) correspond to critical bridges. All these level lines are nonintersecting. (Note that, although these curves emerge from the point  $A$ , no bridge exists that corresponds to the actual point  $A$ .) The slenderness and volume,  $\Lambda$  and  $V$ , increase monotonically, and  $V$  tends to infinity as  $\Lambda \rightarrow \infty$ . Selected lines of constant  $\beta_1$  are presented in Fig. 3. Note that, to ensure high accuracy in construction of the function  $\Omega(\Lambda, V)$ , we used much denser families of the level lines for  $k=1$  and  $k=2$  than those shown in Fig. 3 and in subsequent figures (increments of  $\beta_1$  were between  $0.1^\circ$  and  $1^\circ$ ).

The cylindrical bridge,  $V=1$ , is a singular case. Only cylindrical bridges with  $\Lambda < \pi$  are stable. They correspond to points of the linear segment  $AF$  (Fig. 3). Furthermore, stable states with  $\beta_1 = 90^\circ$  are found only on the segment  $AF$ .

For  $k=1$ , the level lines  $\beta_1 = \text{const}$  that correspond to constricted bridges with  $90^\circ < \beta_1 < 180^\circ$  are more compli-

cated. Each of these lines originates from the point  $A$ , touches the stability boundary at an inner point on the segment  $CE$ , and then turns up and terminates at an inner point on the line  $QGI$ . This is illustrated in Fig. 4(a). That part of the level line between the point  $A$  and the point at which it is tangent to  $CE$  corresponds to stable states. The remainder of the line corresponds to unstable states. Thus the segment  $CE$  of the stability boundary is the envelope of a family of level lines that correspond to  $k=1$  bridges. This finding is consis-

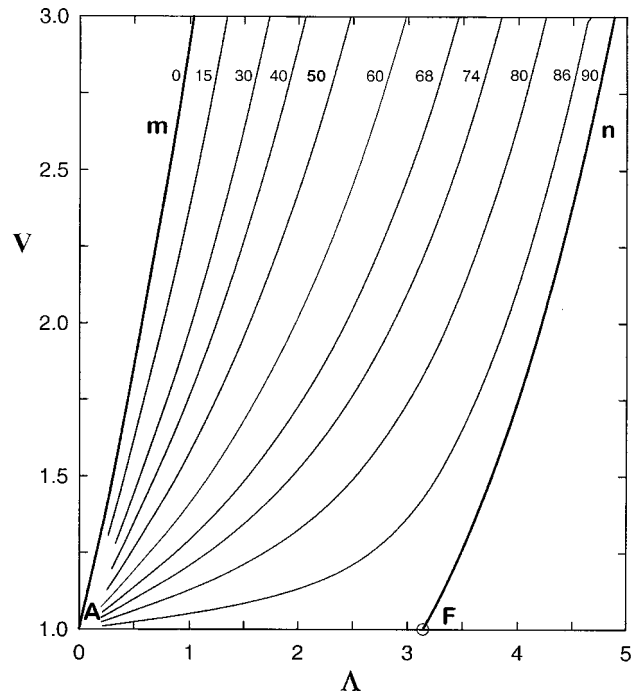


FIG. 3. Selected level lines (thin solid lines)  $\beta_1 = \text{const}$  for the  $k=1$  liquid bridges inside the stability region corresponding to  $V > 1$ . Numbers on curves indicate the  $\beta_1$  values in degrees. Thick solid lines represent boundaries of the stability region and correspond to  $k=1$  liquid bridges with  $\beta_1 = 0$  and  $\beta_1 = 90^\circ$ .

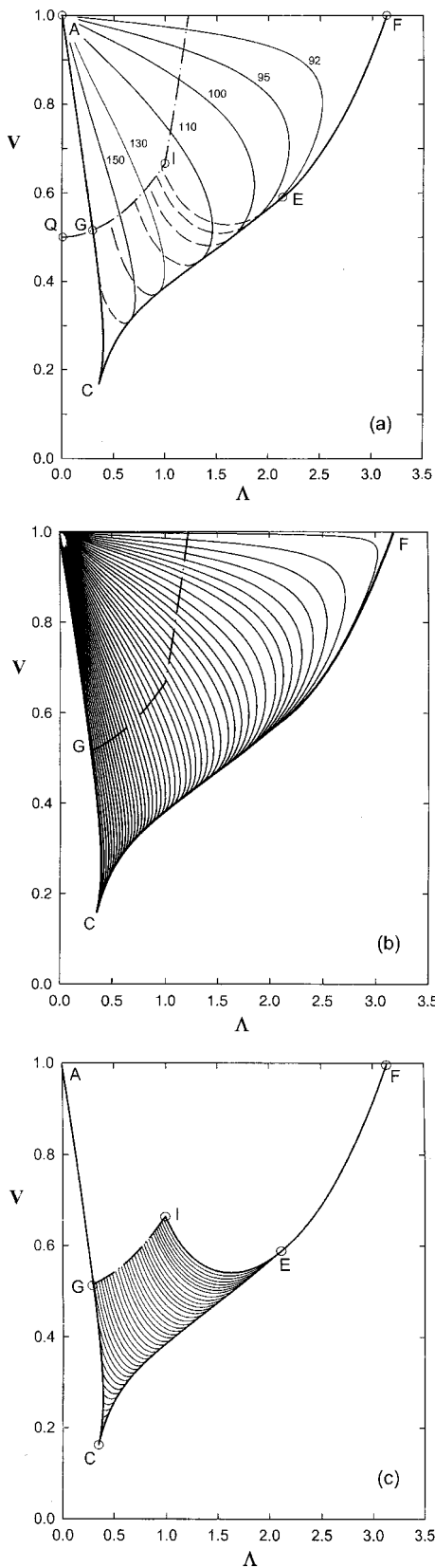


FIG. 4. Level lines  $\beta_1 = \text{const}$  for liquid bridges with  $k=1$  and  $V < 1$ . (a) Selected level lines with  $90^\circ < \beta_1 < 180^\circ$ . Thin solid lines correspond to stable bridges, and dashed lines to unstable bridges. Numbers on curves denote the value of  $\beta_1$  in degrees. Terminal unstable configurations lie on the dot-dash line. The solid thick line is the boundary of the stability region. (b) Dense family of level lines for stable bridges. (c) Dense family of level lines for unstable bridges.

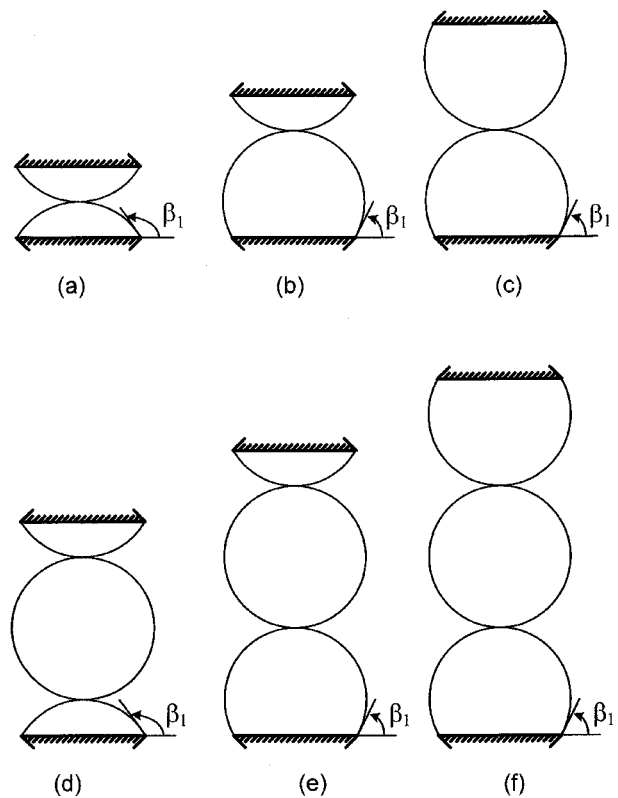


FIG. 5. Bridges consisting of contacting spheres and/or spherical segments that represent limiting configurations for bridges with: (a)  $k=1$ ; (b)  $k=2$ ; (c)  $k=3\{1\}$ ; (d)  $k=3\{2\}$ ; (e)  $k=4$ ; (f)  $k=5\{2\}$ . The number in braces denotes magnitude of the minima on the bridge profile (see Sec. IV A).

tent with a known result<sup>7-11</sup> that the curve  $CE$  is a locus of turning points in volume, i.e., for a fixed  $\Lambda$  ( $0.361 < \Lambda < 2.129$ ), the liquid bridge volume  $V$  reaches a minimum at a point on that curve. Dense families of level lines for stable and unstable bridges are shown separately in Figs. 4(b)–4(c).

Points of the line  $QGI$  correspond to unstable “bridges” that consist of two equal spherical segments that touch each other [Fig. 5(a)]. Along  $QGI$ , the volume of each spherical segment is less than a hemisphere and coincides with a hemisphere only at the point  $I$ . For a bridge consisting of two such spherical segments

$$q = 2 \sin \beta_1, \tag{8}$$

$$\Lambda = (1 + \cos \beta_1) / \sin \beta_1, \tag{9}$$

$$V = (1 + \cos \beta_1)(2 - \cos \beta_1) / (3 \sin^2 \beta_1), \tag{9}$$

$$\Omega = 4 \pi (1 + \cos \beta_1) / \sin^2 \beta_1. \tag{10}$$

Equations (8)–(10) follow from the fact that the dimensionless radius of the base of the spherical segment is unity.

As far as we are aware, Boucher and Jones<sup>9</sup> were the first to point out that a bridge shape corresponding to equidimensional spherical segments in contact represents a limiting case for  $k=1$  liquid bridges with fixed  $\beta_1$ ,  $90^\circ < \beta_1 < 180^\circ$ . Indeed, the contacting spherical surfaces always separate a family of unduloidal surfaces from nodoidal ones. When moving along the level line  $\beta_1 = \text{const}$  from the point  $A$ , the  $q$ -value increases monotonically from  $-\infty$  up to

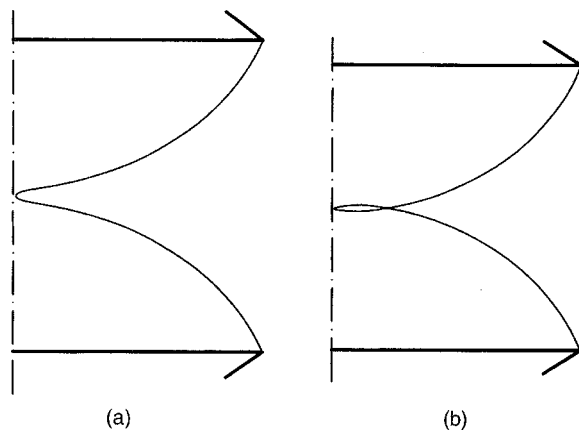


FIG. 6. Profiles of the  $k=1$  unduloidal (a) and nodoidal (b) surfaces with  $\beta_1 = 110^\circ$  separated by the limiting bridge schematically shown in Fig. 5(a). These surfaces correspond to  $q=1.86$  ( $\Lambda=0.754$ ,  $V=0.548$ ) and  $q=1.89$  ( $\Lambda=0.668$ ,  $V=0.605$ ), respectively, while the limiting bridge for  $\beta_1 = 110^\circ$  has  $q=1.879$ ,  $\Lambda=0.700$  and  $V=0.582$ .

$q_{\max} = 2 \sin \beta_1$ . As  $q_{\max}$  is approached from below, the corresponding bridge free surface is an unduloidal surface with a small radius neck [see Fig. 6(a)]. The value  $q_{\max}$  cannot be exceeded because  $q > q_{\max}$  would correspond to a transition to nodoidal surfaces with a self-intersecting profile. Clearly, a self-intersecting profile [Fig. 6(b)] is physically impossible. Thus, there is no unstable bridge with  $k=1$  in the region lying beyond the line  $QGI$ .

The line  $EI$  [Fig. 4(c)] (first constructed by Lowry and Steen<sup>10</sup>) is an extension of the  $EFn$  branch of the stability boundary. In contrast to the line  $EFn$  that corresponds to critical  $k=1$  bridges with  $\beta_1 = 90^\circ$ , the points within  $EI$  correspond to unstable  $k=1$  bridges with  $\beta_1 = 90^\circ$ . Thus each point inside the region  $GIECG$  [Fig. 4(c)] corresponds to one stable and to one unstable  $k=1$  bridge. Figure 7 illustrates shapes of such bridges at the point of intersection of the lines  $\beta_1 = 130^\circ$  (stable states) with the line  $\beta_1 = 110^\circ$  (unstable states) [see Fig. 4(a); later this point will be denoted by "1" in Fig. 9(a)]. From following discussion it will become clear that the only unstable bridges in the region  $GIECG$  are  $k=1$  axisymmetric bridges.

One of the most important bridge configurations has a catenoidal profile. The catenoids are characterized with the equality  $q=0$ . They always have  $k=1$  and exist only for  $\Lambda \leq 0.6627$ . The basic results on the stability of catenoid configurations were obtained by Erle *et al.*<sup>14</sup> For a given  $\Lambda < 0.6627$ , there are two catenoids corresponding to two values of  $V$ . The one corresponding to the largest  $V$  is always stable. The other is stable if  $0.4718 < \Lambda < 0.6627$ , and unstable if  $\Lambda < 0.4718$ . Stable catenoids are located within the segment  $AWD$  (Fig. 8). The segment  $AWD$  touches the stability boundary at the point  $D$  that corresponds to a critical catenoid. The catenoid with a maximum slenderness  $\Lambda = 0.6627$  has a relative volume  $V = 0.5$ . The point of intersection of the locus of catenoids with a given level line  $\beta_1 = \text{const}$  corresponds to a catenoid with a prescribed  $\beta_1$ . The relationship between  $\Lambda$  and  $\beta_1$  for catenoids is presented in Ref. 9.

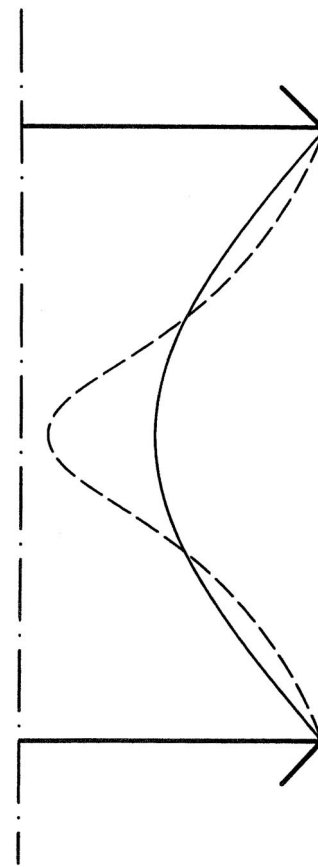


FIG. 7. Profiles of stable (solid line) and unstable (dashed line) bridges corresponding to  $\Lambda=0.99$  and  $V=0.46$ . For these bridges,  $\beta_1 = 130^\circ$ ,  $q = 0.800$ ,  $\Omega = 9.68$  and  $\beta_1 = 110^\circ$ ,  $q = 1.722$ ,  $\Omega = 10.04$ , respectively.

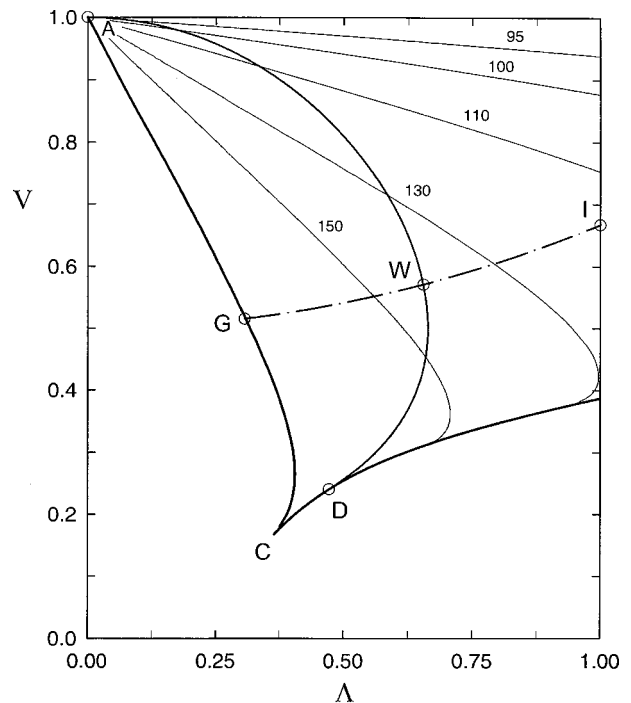


FIG. 8. Locus  $AWD$  of stable catenoidal configurations. Thin solid lines relate to the level lines  $\beta_1 = \text{const}$  for stable bridges.

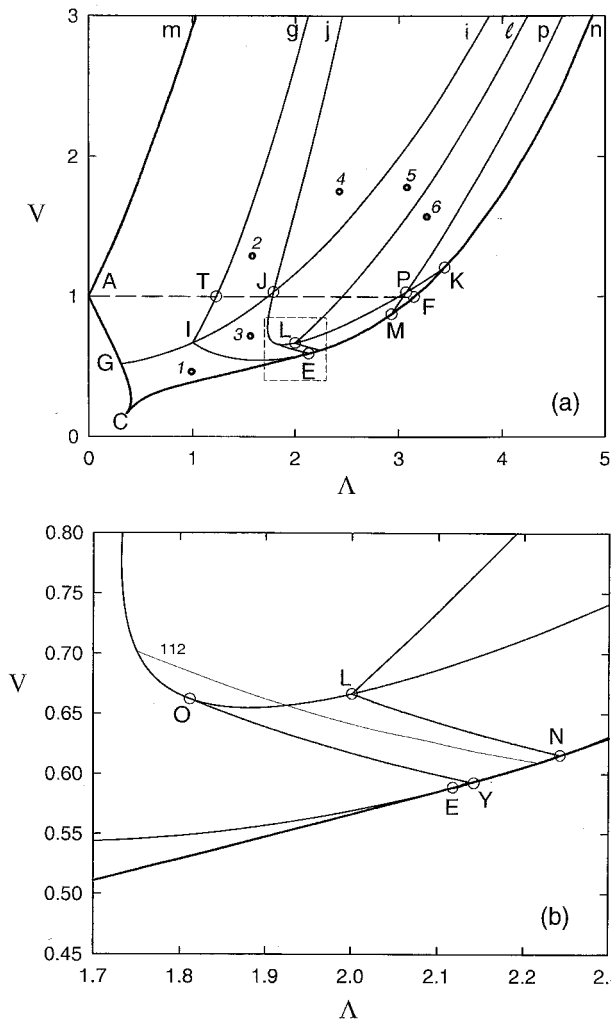


FIG. 9. (a) Map of regions with different types of unstable axisymmetric bridges. (b) A fragment corresponding to the segment *JL*.

**B. Unstable  $k=2$  bridges**

The segment *GI* has a smooth continuation *IJi* across the point *I* [see Fig. 9(a)]. We will discuss this continuation later. First we consider the branch *ITg* that bifurcates at the point *I*. Points of this branch correspond to unstable bridges that consist of two unequal spherical segments that touch. The two segments are the complements to a sphere [Fig. 5(b) or an identical configuration that is inverted]. As was noted by Haynes<sup>12</sup> and by Boucher and Jones,<sup>9</sup> such a bridge represents the terminal configuration for the unduloidal  $k=2$  family of unstable bridges. As this configuration is approached, the point of maximum of  $r(s)$  for the  $k=2$  bridge profile approaches the maximum radius of a circular section of the larger spherical segment and the point of minimum of  $r(s)$  approaches the point at which the spherical segments are tangent.

When moving along the line *ITg* in the direction away from the point *I*, the angle  $\beta_1$  for a bridge consisting of two spherical segments changes monotonically from the value  $90^\circ$ . [For the configuration shown in Fig. 5(b),  $\beta_1$  decreases. It increases for the inverted configuration.] Points of the branch *ITg* are determined as

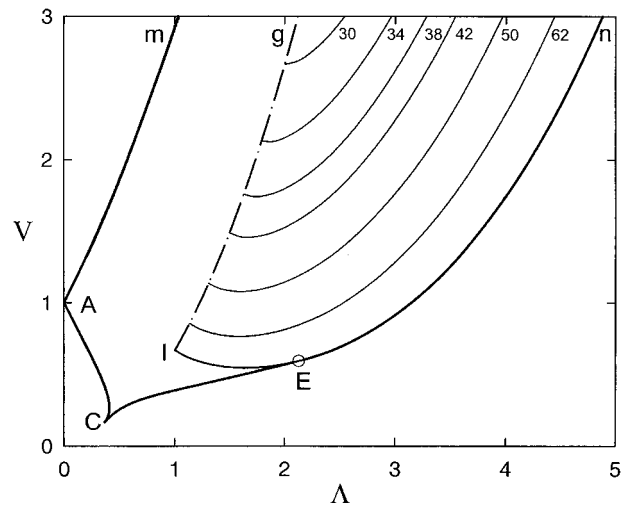


FIG. 10. Selected level lines  $\beta_1 = \text{const}$  for liquid bridges with  $k=2$ . Numbers on curves indicate the values of  $\beta_1$  in degrees.

$$\Lambda = 1/\sin \beta_1, \quad V = 2/(3 \sin^2 \beta_1). \tag{11}$$

The free surface area for such a bridge is

$$\Omega = 4\pi/\sin^2 \beta_1, \tag{12}$$

and the  $q$ -value is determined by Eq. (8).

Unstable  $k=2$  bridges exist only in the open region *gTIEMFKn* [Fig. 9(a)]. Figure 10 illustrates the behavior of the level lines  $\beta_1 = \text{const}$  for bridges with  $k=2$ . Bridges with  $k=2$  cannot exist to the left of the branch *ITg* by the same reasoning as for unstable  $k=1$  bridges limited by the configurations on the line *QGI*. On the other hand, we see that the level line  $\beta_1 = a$  for  $k=2$  bridges tends to the line *IEMFKn* as  $a \rightarrow 90^\circ$ , so that the level lines  $\beta_1 = a$  with  $0 < a < 90^\circ$  fill the region *gTIEMFKn*. Since bridges with  $\beta_1 = a$  and with  $\beta_1 = 180^\circ - a$  are identical for even  $k$  (they are rotated through  $180^\circ$  relative to each other), the lines  $\beta_1 = a$  and  $\beta_1 = 180^\circ - a$  coincide and the level lines  $\beta_1 = a$  with  $90^\circ < a < 180^\circ$  show no new information.

The line *IEMFKn* is simultaneously the level line  $\beta_1 = 90^\circ$  for  $k=1$  bridges and a limit for lines  $\beta_1 = a$  ( $k=2$ ) as  $a \rightarrow 90^\circ$ . This serves as an illustration of the known fact<sup>10</sup> that the  $k=2$  bridges bifurcate from critical axisymmetric bridges belonging to the boundary branch *EMFKn* and from unstable  $k=1$  bridges belonging to the segment *IE*.

As an example, Fig. 11 shows the profiles of stable and unstable bridges that correspond to the point  $\Lambda = 1.577, V = 1.296$  [it is denoted by “2” in Fig. 9(a)]. This point is the point of intersection of the level lines  $\beta_1 = 77^\circ$  for stable  $k=1$  bridges and  $\beta_1 = 45^\circ$  for unstable  $k=2$  bridges.

**IV. UNSTABLE  $k>2$  AXISYMMETRIC BRIDGES: DOMAINS OF EXISTENCE**

As was shown in Refs. 9 and 10, several unstable axisymmetric bridges may correspond to the same point of the stability region in the  $(\Lambda, V)$  plane. Here we extend these results by construction the domains of existence for all possible bridges with  $k \geq 3$ .

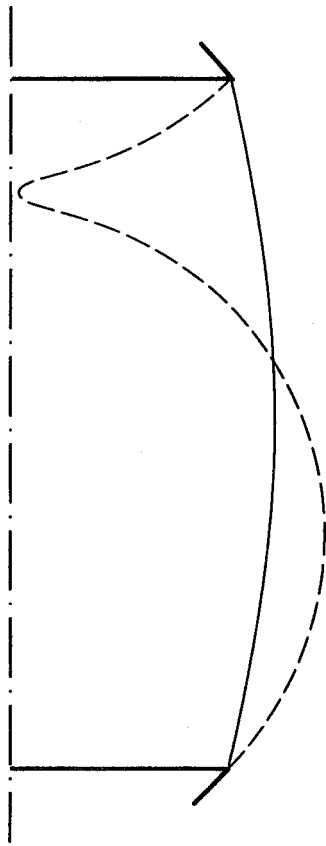


FIG. 11. Profiles of liquid bridges with  $\Lambda=1.577$  and  $V=1.296$ . The solid line corresponds to a  $k=1$  stable bridge ( $\beta_1=77^\circ$ ,  $q=1.015$ ,  $\Omega=22.77$ ), and the dashed line to a  $k=2$  unstable bridge ( $\beta_1=45^\circ$ ,  $q=1.365$ ,  $\Omega=26.54$ ).

**A. Unstable bridges with  $k=3$  (1 point of minimum and 2 points of maximum)**

Let us reconsider the branch  $IJi$  [Fig. 9(a)] that represents a smooth continuation of the segment  $GI$ . All points of  $IJi$  correspond to bridges that consist of two equal spherical segments. In contrast to the line  $GI$ , each of spherical segments within  $IJi$  is greater in volume than a hemisphere [Fig. 5(c)] and is coincident with a hemisphere only at the point  $I$ . When moving along the line  $IJi$  in the direction away from  $I$ , the angle  $\beta_1$  for such a bridge monotonically decreases from the value  $90^\circ$  at the point  $I$ . Equalities (8)–(10) still hold for bridges corresponding to points on  $IJi$  that are comprised of two spherical segments.

A bridge formed by the above spherical segments is a limiting case of unstable unduloidal bridges with surface profiles that contain three extreme points ( $k=3$ ) of  $r(s)$ . One of them is a minimum, and two others are maxima.<sup>9</sup> For odd wave numbers, we denote the number of minima in a profile by the number in curly braces, e.g.,  $k=3\{1\}$ . This kind of bridge exists both inside and outside the stability region. Inside, the domain of existence is bounded by  $iJIEMFKn$ . Selected lines of  $\beta_1=\text{const}$  for bridges with  $k=3\{1\}$  are shown in Fig. 12. Each of these lines can be extended beyond the point of intersection with the boundary segment  $EMFKn$ .

Thus, each point of the domain  $iJIEMFKn$  corresponds

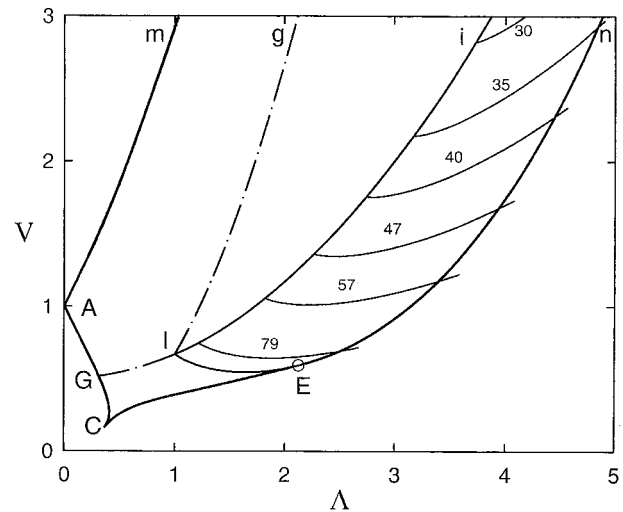


FIG. 12. Level lines  $\beta_1=\text{const}$  for liquid bridges with  $k=3\{1\}$  (thin solid lines). Numbers on curves denote the values of  $\beta_1$  in degrees.

to at least three bridges: to a stable bridge, to an unstable  $k=2$  bridge, and to an unstable bridge with  $k=3\{1\}$ . Figure 13 shows the profiles of bridges that correspond to the point denoted by “3” in Fig. 9(a). For a given pair  $\Lambda$  and  $V$ , the values  $\beta_1$  and  $q$  for different  $k$  are determined iteratively.

**B. Unstable bridges with  $k=3\{2\}$ ,  $k=4$ ,  $k=5\{2\}$ , and  $k=5\{3\}$**

Under examination the bifurcations at  $\Lambda=1.75, 2, 2.5$  and  $\pi$ , Lowry and Steen<sup>10</sup> have analyzed more complicated axisymmetric bridges with  $k=3\{2\}$ , 4 and  $5\{2\}$ . Here we will determine the domains within the stability region where these bridges exist. To do this we use Lowry and Steen’s<sup>10</sup> idea that the limiting configurations for such bridges represent different combinations of a sphere in contact with two spherical segments of the same radius [Figs. 5(d)–5(f)]. Such bridges with two equidimensional symmetric spherical segments belong to the branch  $jJLPK$  [Fig. 9(a)]. Along  $jJL$ , these bridges have the angle  $\beta_1 > 90^\circ$  [Fig. 5(d)], and they represent a limiting case for unstable bridges with  $k=3\{2\}$ . Within  $LPK$ , the bridges formed by spheres have the initial slope  $\beta_1 < 90^\circ$  [Fig. 5(f)], and they represent the terminal configuration for unstable bridges with  $k=5\{2\}$ . The equation of the branch  $jJLPK$  can be written in the form

$$\Lambda = \frac{2 + \cos \beta_1}{\sin \beta_1}, \quad V = \frac{2 + (2 - \cos \beta_1)(1 + \cos \beta_1)^2}{3(2 + \cos \beta_1)\sin^2 \beta_1}. \tag{13}$$

The point  $L$  in Fig. 9 corresponds to  $\beta_1=90^\circ$  and represents the bifurcation point for bridges that consist of a sphere and two spherical segments. The branch  $Ll$  corresponds to bridges that consist of a sphere and two unequal spherical segments that complement a full sphere [Fig. 5(e)]. These bridges represent a limiting case for  $k=4$ . Along the branch  $Ll$ ,

$$\Lambda = 2/\sin \beta_1, \quad V = 2/(3 \sin^2 \beta_1). \tag{14}$$

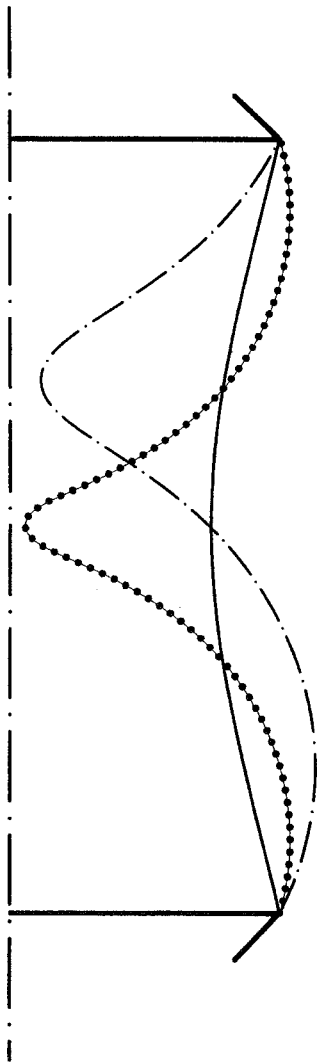


FIG. 13. Surface profiles for bridges with  $\Lambda=1.562$  and  $V=0.715$ . The solid line corresponds to a  $k=1$  stable bridge ( $\beta_1=102.4^\circ$ ,  $q=1.043$ ,  $\Omega=16.79$ ), the dot-dash line to a  $k=2$  bridge ( $\beta_1=65^\circ$ ,  $q=1.610$ ,  $\Omega=17.93$ ), and the dotted line to a  $k=3\{1\}$  bridge ( $\beta_1=75^\circ$ ,  $q=1.836$ ,  $\Omega=18.16$ ).

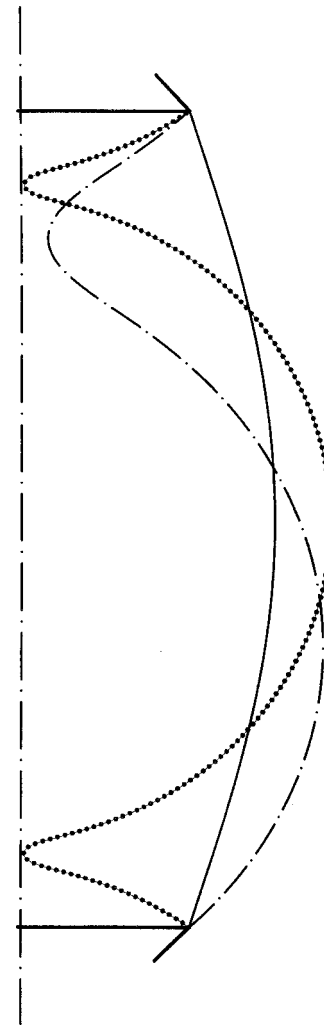


FIG. 14. Profiles of axisymmetric bridges with  $\Lambda=2.42$  and  $V=1.75$ . The solid line corresponds to a  $k=1$  stable bridge ( $\beta_1=73.3^\circ$ ,  $q=0.87$ ,  $\Omega=40.93$ ), the dot-dash line to a  $k=2$  bridge ( $\beta_1=42^\circ$ ,  $q=1.033$ ,  $\Omega=43.64$ ), and the dotted line to a  $k=3\{2\}$  bridge ( $\beta_1=145^\circ$ ,  $q=1.085$ ,  $\Omega=48.99$ ).

For a given  $V$ , the value of  $\Lambda$  along the branch  $Ll$  is twice that along  $ITg$  [compare Eq. (14) with (11)].

Unstable bridges with  $k=3\{2\}$  exist in the open domain  $jJOYNMFKn$  [Figs. 9(a)–9(b)]. The segment  $OY$  [Fig. 9(b)] corresponds to bridges with  $\beta_1=105^\circ$ . This is the lowest level line  $\beta_1=\text{const}$  for the  $k=3\{2\}$  bridges. The segment  $LN$  represents the line  $\beta_1=90^\circ$ . It should be noted that, each point inside the region  $OYNLO$  corresponds to two  $k=3\{2\}$  bridges. For one, the value of  $\beta_1$  lies between  $90^\circ$  and  $105^\circ$ . The related level line  $\beta_1=\text{const}$  through a given point originates from a point within the segment  $OL$ . The other bridge corresponds to  $\beta_1$  greater than  $105^\circ$ . The corresponding level line starts from some point on the segment  $OJ$  [see the line  $\beta_1=112^\circ$  shown in Fig. 9(b)]. Figure 14 illustrates all possible axisymmetric bridges at the point denoted by “4” in Fig. 9(a).

Three unstable bridges exist in the open domain  $iJLL$ . Figure 15 shows shapes of bridges corresponding to the point denoted by “5” in Fig. 9(a). Unstable bridges with  $k=4$  exist in the open domain  $ILNMFKn$  [Figs. 9(a)–9(b)]. A

stable bridge and four unstable bridges that correspond to the point “6” in Fig. 9(a) are shown in Fig. 16. Finally, the domain  $KPLNMFKn$  contains the unstable  $k=5\{2\}$  bridges.

Cases of unstable bridges with a higher wave number can be considered in similar manner. For example, to obtain the regions of existence of unstable bridges with  $k=5\{3\}$ ,  $k=6$ , and  $k=7\{3\}$  we have to analyze the configurations like that presented in Figs. 5(d)–5(f), but with two (not one) full spheres. Our analysis has shown that only unstable bridges with  $k=5\{3\}$  can exist inside the stability region. The domain of existence is the open region  $pPMFKn$  [Fig. 9(a)]. The branch  $Mpp$  corresponds to unstable bridges formed by two full spheres in contact with two symmetric spherical segments of the same radius with  $\beta_1 > 90^\circ$ . Along this branch,

$$\Lambda = \frac{3 + \cos \beta_1}{\sin \beta_1}, \quad V = \frac{4 + (2 - \cos \beta_1)(1 + \cos \beta_1)^2}{3(3 + \cos \beta_1)\sin^2 \beta_1}. \tag{15}$$

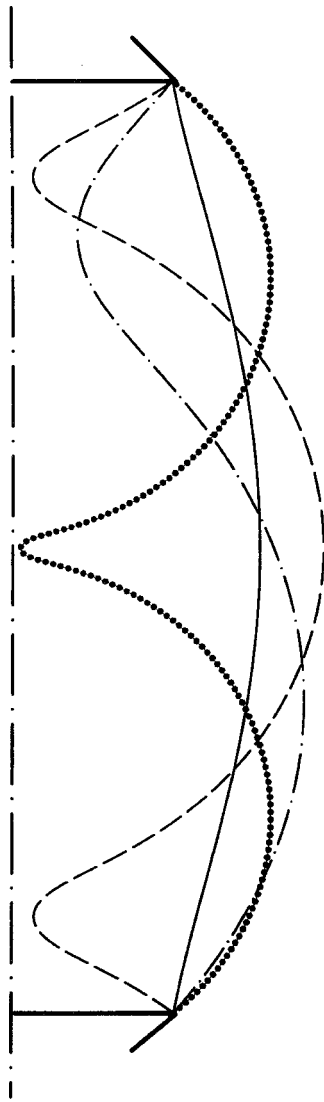


FIG. 15. Surface profiles for liquid bridges with  $\Lambda=3.07$  and  $V=1.78$ . Solid line: a  $k=1$  stable bridge ( $\beta_1=80^\circ$ ,  $q=0.811$ ,  $\Omega=51.91$ ); dot-dash line: a  $k=2$  bridge ( $\beta_1=51^\circ$ ,  $q=0.908$ ,  $\Omega=52.97$ ); dotted line: a  $k=3\{1\}$  bridge ( $\beta_1=40^\circ$ ,  $q=1.222$ ,  $\Omega=58.83$ ); and dashed line: a  $k=3\{2\}$  bridge ( $\beta_1=143.2^\circ$ ,  $q=0.976$ ,  $\Omega=57.48$ ).

Unstable bridges with  $k \geq 6$  do not exist inside the stability region bounded by thick solid lines in Fig. 9(a). The domains of existence of different types of axisymmetric unstable bridges are summarized in Table II.

Expressions for  $\Omega$  can also be easily written for all these “limiting” spherical configurations discussed here. Note that the value of  $q$  is always given by  $2 \sin \beta_1$ .

### V. POINT OF EMERGENCE FROM THE POTENTIAL WELL

In the preceding sections we found that there is one unstable ( $k=1$ ) axisymmetric state at any point of the region  $GCEIG$  and there are one ( $k=2$ ) or more unstable axisymmetric states within the region  $gTIEMFKn$  [Fig. 9(a)]. For a fixed  $\Lambda < 1$  ( $\Lambda=1$  at the point  $I$ ), only a branch of the  $k=1$  bridges exists. Lowry and Steen<sup>10</sup> have shown that at fixed  $\Lambda > 1$ , the  $k=1$  branch is connected only with the  $k=2$  and

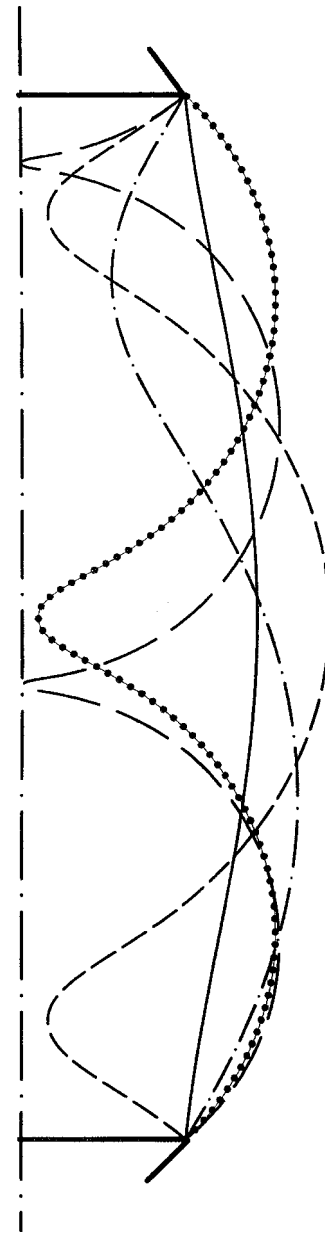


FIG. 16. Profiles of bridges associated with  $\Lambda=3.26$  and  $V=1.57$ . A stable  $k=1$  bridge (solid line,  $\beta_1=85^\circ$ ,  $q=0.832$ ,  $\Omega=51.56$ ); a  $k=2$  bridge (dot-dash line,  $\beta_1=60^\circ$ ,  $q=0.899$ ,  $\Omega=51.97$ ); a  $k=3\{1\}$  bridge (dotted line,  $\beta_1=45^\circ$ ,  $q=1.216$ ,  $\Omega=56.32$ ), a  $k=3\{2\}$  bridge (short-dashed line,  $\beta_1=139.5^\circ$ ,  $q=0.988$ ,  $\Omega=55.68$ ), and a  $k=4$  bridge (long-dashed line,  $\beta_1=40.3^\circ$ ,  $q=1.272$ ,  $\Omega=61.71$ ).

$k=3\{1\}$  branches (except for the singular value of  $\Lambda=4.5465$ ). This means that the point of emergence from the potential well for a stable state (recall that  $k=1$  for stable states) cannot be determined by the axisymmetric states with  $k=3\{2\}$  or  $k \geq 4$ . Furthermore, the structure of the family of branches  $k=1, 2, 3\{1\}$  shows that states with  $k=3\{1\}$  also cannot serve as the points of emergence. For a stable state with  $1 < \Lambda < 2.129$  (where 2.129 is value of  $\Lambda$  at the point  $E$ ), the point of emergence is determined by an unstable  $k=1$  bridge if  $V$  is less than that associated with the line  $IE$  [Fig. 9(a)]. Along  $IE$ , the  $k=2$  bridges bifurcate from unstable  $k=1$  bridges in the direction of increasing  $V$ . When crossing

TABLE II. Unstable axisymmetric bridges that exist in different parts of the stability region shown in Fig. 9.

Subregion	Wave number $k$
<i>GCEIG</i>	1
<i>gTIJj</i>	2
<i>JIEYOJ</i>	2, 3{1}
<i>jJi</i>	2, 3{2}
<i>iJOLI</i>	2, 3{1}, 3{2}
<i>OYNLO</i>	2, 3{1}, 3{2}, 3{2}
<i>lLPp</i>	2, 3{1}, 3{2}, 4
<i>pPKn</i>	2, 3{1}, 3{2}, 4, 5{3}
<i>PLNMP</i>	2, 3{1}, 3{2}, 4, 5{2}
<i>PMKP</i>	2, 3{1}, 3{2}, 4, 5{2}, 5{3}

the line *IE* from below, the  $k=2$  bridges replace the unstable  $k=1$  bridges at the point of emergence despite the fact that the  $k=3\{1\}$  bridges serve as a smooth continuation of the unstable  $k=1$  bridges across the line *IE*. When  $\Lambda \geq 2.129$ , there are no unstable  $k=1$  bridges. Here the  $k=2$  bridges bifurcate from critical  $k=1$  bridges toward subcritical region. The  $k=3\{1\}$  bridges first bifurcate outside the stability region, so again the  $k=2$  bridges serve as the emergence point.

Thus, for axisymmetric states, we can draw the conclusion that the point of emergence from the potential well is determined by the  $k=1$  unstable bridge within the domain *GCEIG*, and by the bridge with  $k=2$  in the domain *gTIEMFKn*. However, we cannot rule out the possibility that, under variation of the parameters  $\Lambda$  and  $V$ , nonaxisymmetric shapes branch off from unstable  $k=1$  or  $k=2$  axi-

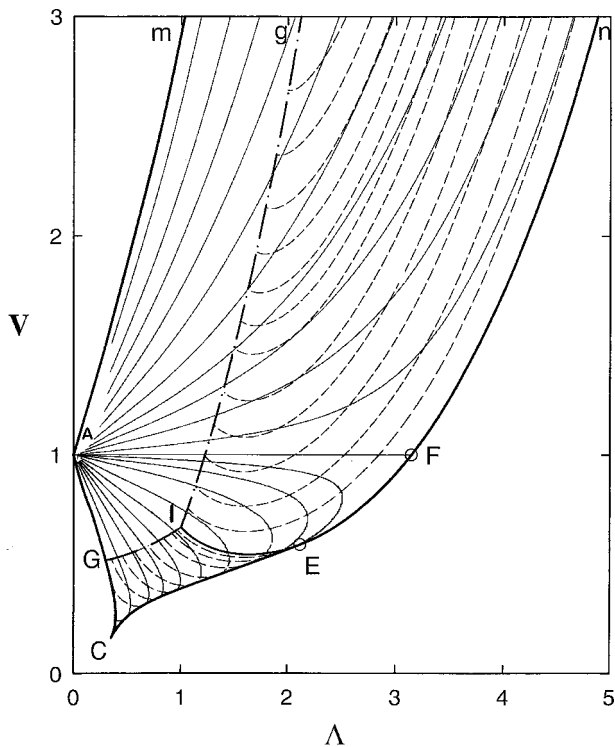


FIG. 17. Superposition of level lines  $\beta_1 = \text{const}$  for  $k=1$  stable bridges (solid lines) and level lines  $\beta_1 = \text{const}$  for  $k=1$  and  $k=2$  unstable bridges (dashed lines).

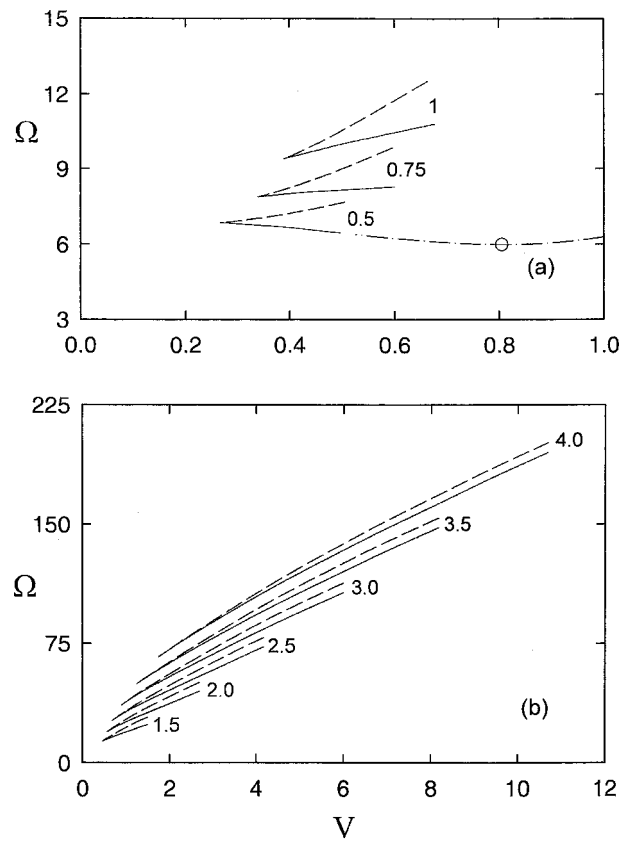


FIG. 18. Dimensionless free surface area,  $\Omega$ , as a function of the relative volume,  $V$ , for stable (solid line) and unstable (dashed line) bridges ( $k=1$  or  $k=2$ ) and fixed  $\Lambda$ . Numbers on curves indicate the value of  $\Lambda$ .

symmetric bridges. In this case, the bifurcating nonaxisymmetric bridge may serve as the emergence point and determine the stability margin. To investigate this, we have to examine the stability with respect to nonaxisymmetric perturbations of  $k=1$  and  $k=2$  axisymmetric bridges that are already unstable to axisymmetric perturbations. If they are stable, then there are no bifurcating nonaxisymmetric bridges. According to the method described by Myshkis *et al.*,<sup>4</sup> a bridge is stable to nonaxisymmetric perturbations if the function  $\varphi(s)$  does not change its sign in the interval  $0 < s \leq s^*$ , where  $\varphi(s)$  is the solution of the following problem:

$$\varphi'' + \frac{r'}{r} \varphi' + \left( \beta'^2 - \frac{r'^2}{r^2} \right) \varphi = 0,$$

$$\varphi(0) = 0, \quad \varphi'(0) = 1, \quad \left( ' = \frac{d}{ds} \right). \quad (16)$$

Our systematic calculations have shown that the function  $\varphi(s)$  is always positive in the interval  $0 < s \leq s^*$  for all unstable  $k=1$  and  $k=2$  bridges under consideration.

Consequently, neither  $k=1$  bridges that are unstable to axisymmetric perturbations, nor  $k=2$  bridges lose the stability to nonaxisymmetric perturbations. Thus, these bridges determine the points of emergence from potential wells for stable states within the domains *GCEIG* and *gTIEMFKn*, respectively. Figure 17 is a combination of data presented in

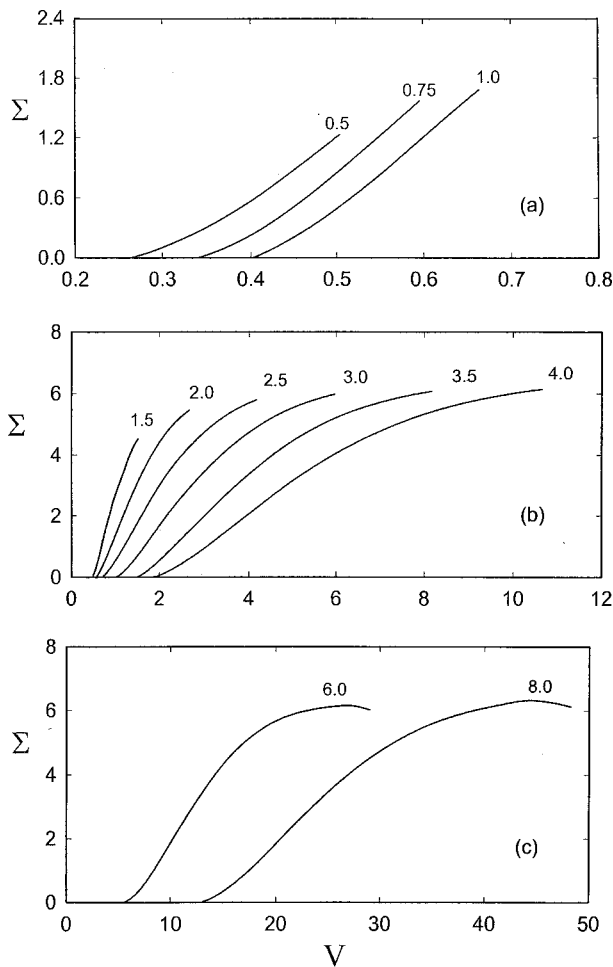


FIG. 19. Dimensionless stability margin,  $\Sigma$ , as a function of the relative volume,  $V$ , for different fixed  $\Lambda$  indicated by numbers on curves: (a) short bridges; (b) medium length bridges; (c) long bridges.

Figs. 3, 4, and 10 and shows level lines for stable bridges coupled with those for bridges corresponding to the point of emergence.

**VI. THE STABILITY MARGIN**

The dimensionless surface areas (potential energy) of stable bridges and unstable bridges with  $k=1$  or  $k=2$  for several fixed  $\Lambda$  are shown in Fig. 18. The terminating  $V$  value for each  $\Lambda$  (except for  $\Lambda=0.5$ ) is determined by the corresponding value on the curve  $GITg$ . Boucher and Jones<sup>9</sup> have shown that there are extreme points on curves related to  $\Lambda < 0.6627$ . These points correspond to catenoidal free surfaces. In particular, the point of minimum on the curve for stable states (see the curve for  $\Lambda=0.5$  extended by the dot-dash line beyond the  $V$  value on the segment  $GI$ ) corresponds to the stable catenoid located on the branch related to a larger value of  $V$  for a given  $\Lambda$  (see Fig. 8). Extreme points are absent on the curves corresponding to  $\Lambda > 0.6627$ .

The dimensionless stability margin,  $\Sigma$ , calculated for bridges with fixed  $\Lambda$  is shown in Fig. 19. Note that  $\Sigma$  increases with  $V$  for short and medium length bridges [Figs. 19(a)–19(b)]. For small  $\Lambda$ , the curve  $\Sigma(V)$  is steeply inclined. However, as  $\Lambda$  increases, the curve slopes more gen-

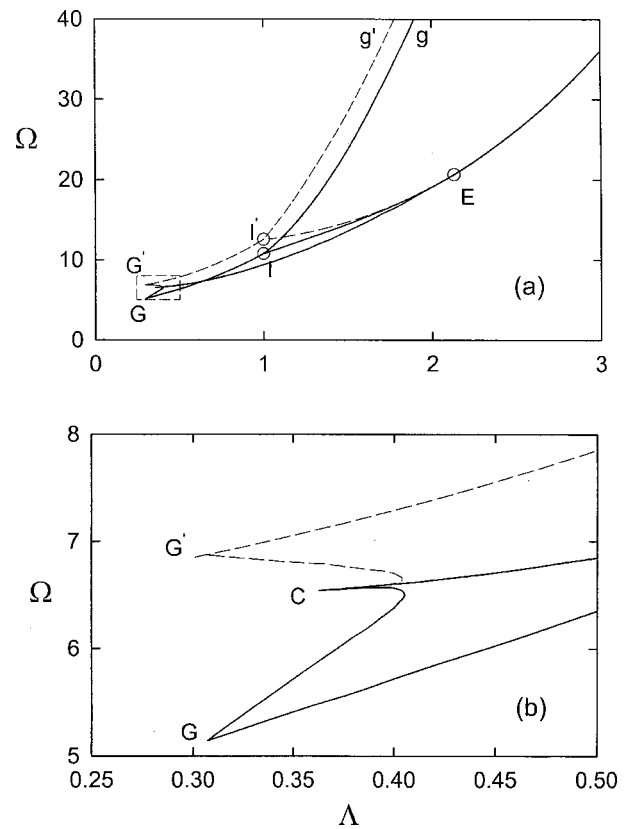


FIG. 20. Dimensionless area,  $\Omega$ , as a function of slenderness,  $\Lambda$ , for stable (solid line) and unstable (dashed line) bridges along the segments  $CG$ ,  $GI$ ,  $Ig$ , and  $IE$ . Designations for stable states are the same as in Fig. 9. Points corresponding to unstable states are “primed.”

tly. This effect is most evident as the value of  $V$  at the terminating configuration is approached [Fig. 19(b)].

Thus, for a fixed small and moderate  $\Lambda$ , the stability margin attains its largest value at stable state that belongs to the branch  $GITg$ . Therefore, the stability margin along  $GITg$  is of specific interest. Figure 20 illustrates the values of  $\Omega$  for stable and unstable states along the segments bounding the regions where unstable  $k=1$  or  $k=2$  bridges exist. Figure 21 shows the stability margin along these segments. For moderate  $\Lambda$ , the stability margin along  $ITg$  has only a slight dependence on  $\Lambda$ . For example, it is equal to 5.98, 6.07, and 6.10 when  $\Lambda=3$ , 3.5, and 4, respectively.

The stability margin along  $CDEFn$  is zero because this segment corresponds to bridges that are critical to axisymmetric perturbations. However, we assume that this is not true for the segment  $GC$ . To obtain the stability margin along  $GC$  (Fig. 21) we consider the associated states with  $\beta_1=180^\circ$  (which are critical to nonaxisymmetric perturbations) as the states stable to axisymmetric perturbations and compare them with unstable  $k=1$  axisymmetric bridges that belong to this segment [see Fig. 4(c)].

Of particular interest are the stability margins for stable cylindrical and catenoidal bridges. They are also shown in Fig. 21. For cylindrical bridges ( $V=1$ ), the stability margin is determined within the straight-line segment  $TF$  [Fig. 9(a)] that corresponds to  $\sqrt{3}/2 \leq \Lambda \leq \pi$ . For  $V=1$ , the magnitude of the stability margin decreases with increasing bridge slen-

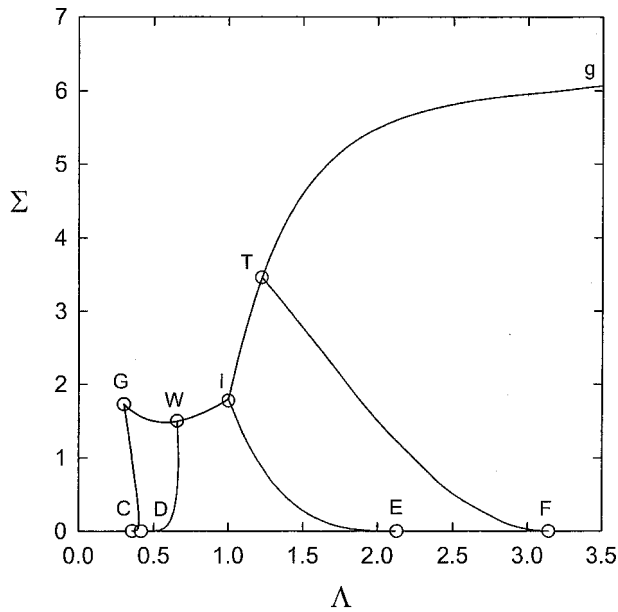


FIG. 21. Dimensionless stability margin,  $\Sigma$ , along the boundary segments  $CG$ ,  $GI$ ,  $ITg$ , and  $IE$ , and for stable cylinders (segment  $TF$ ) and stable catenoids (segment  $WD$ ). The point designations are the same as those used in Figs. 8 and 9.

derness, as would be expected. In particular,  $\Sigma$  decreases from  $(6 - 4\sqrt{3/2})\pi = 3.459$  at  $\Lambda = \sqrt{3/2}$  [see Eqs. (11)–(12)] to 0 at  $\Lambda = \pi$ . The values of  $\Sigma$  for stable cylinders with  $\sqrt{3/2} \leq \Lambda \leq \pi$  have been collected in Table III.

For stable catenoidal bridges associated with the segment  $WD$  (Fig. 8), the values of  $\Omega = \Omega_s$  were compared with the related values of  $\Omega_e$ . It is easy to prove that among all catenoids the area  $\Omega$  has a maximum value of 7.5378 for the catenoid with  $\Lambda = \Lambda_{max} = 0.6627$ . The  $\Omega_e$  values are determined by unstable states corresponding to points of intersection of the level lines shown in Fig. 4(c) with the locus of catenoids (Fig. 8). The value of  $\Sigma$  decreases from 1.4988 at the point  $W$ , to 0 at the point  $D$ . The stability margin data for catenoidal bridges are presented in Table IV. Note that these data are distinctly different from those for soap-film bridges.<sup>5</sup> Film bridges stretched between two open end-rings have only catenoidal equilibrium shapes. For a given  $\Lambda < 0.6627$  they are stable on the branch corresponding to the largest  $V$ , and unstable on the branch with smallest  $V$  (see Fig. 8), so that, in contrast to catenoidal liquid bridges, the limiting catenoid with  $\Lambda = 0.6627$  is critical. Film bridges have no constant-volume constraint, and for a given  $\Lambda < 0.6627$  the stability margin is a free energy difference between corresponding unstable and stable catenoids.

Finally, the lines of equal values of the dimensionless stability margin shown in Fig. 22 help to imagine the surface  $\Sigma(\Lambda, V)$  for  $\Lambda \leq 4$ .

The simple form of the surface  $\Sigma(\Lambda, V)$  for small and moderate  $\Lambda$  becomes somewhat complicated for long bridges. The value of  $\Sigma$  for fixed large values of  $\Lambda$  attains its maximum at the volume  $V$  less than the volume corresponding to the point on  $Ig$  [Fig. 19(c)]. For  $\Lambda = 6$  and 8, the maximum values of  $\Sigma$  are 6.20 and 6.25.

TABLE III. Dimensionless stability margin for cylindrical bridges.

$\Lambda$	$\Sigma$	$\Lambda$	$\Sigma$
1.2247	3.459	2.20	1.075
1.25	3.400	2.25	0.972
1.30	3.280	2.30	0.869
1.35	3.159	2.35	0.767
1.40	3.030	2.40	0.667
1.45	2.901	2.45	0.584
1.50	2.771	2.50	0.510
1.55	2.642	2.55	0.443
1.60	2.513	2.60	0.382
1.65	2.383	2.65	0.326
1.70	2.254	2.70	0.270
1.75	2.125	2.75	0.215
1.80	1.996	2.80	0.161
1.85	1.867	2.85	0.112
1.90	1.744	2.90	0.077
1.95	1.623	2.95	0.048
2.00	1.504	3.00	0.026
2.05	1.390	3.05	0.011
2.10	1.281	3.10	0.003
2.15	1.178	$\pi$	0

### VII. CONCLUSIONS AND DISCUSSION

The stability margin problem for axisymmetric liquid bridges spanning equal disks under zero gravity has been considered using an approach based on finding the finite height potential energy barrier that must be exceeded for the bridge to lose stability. The domain of the stability region in the  $(\Lambda, V)$  plane has been analyzed where unstable axisymmetric liquid bridges coexist with stable ones. This domain ( $gTIGCEMFKn$  in Fig. 9) represents a “strip” of finite width that extends in the  $V$ -direction. It is adjacent to the minimum volume stability limit ( $CEMFKn$ ) and extends into the region  $\Lambda > 0.308$ . The maximum volume boundary ( $GITg$ ) of the strip is determined by a simple analytical expression.

Within the strip, the stability margin is calculated for bridges with  $\Lambda \leq 8$ , and detailed data are obtained for  $\Lambda \leq 4$ . The stability margin first increases with distance from the minimum volume stability limit as would be expected. In

TABLE IV. Dimensionless stability margin for catenoidal bridges.

$\Lambda$	$V$	$\Sigma$	$\Lambda$	$V$	$\Sigma$
0.6536	0.571	1.499	0.610	0.349	0.141
0.656	0.561	1.392	0.600	0.336	0.106
0.658	0.551	1.311	0.590	0.325	0.079
0.660	0.539	1.220	0.580	0.315	0.058
0.662	0.520	1.107	0.570	0.306	0.041
0.6627	0.500	0.963	0.560	0.298	0.029
0.662	0.480	0.836	0.550	0.290	0.020
0.660	0.463	0.733	0.540	0.282	0.013
0.658	0.451	0.650	0.530	0.275	0.008
0.656	0.442	0.600	0.520	0.269	0.006
0.654	0.435	0.555	0.510	0.262	0.004
0.652	0.428	0.512	0.500	0.256	0.003
0.650	0.422	0.472	0.490	0.250	0.002
0.640	0.397	0.350	0.480	0.245	0.001
0.630	0.378	0.260	0.4718	0.2405	0
0.620	0.362	0.193			

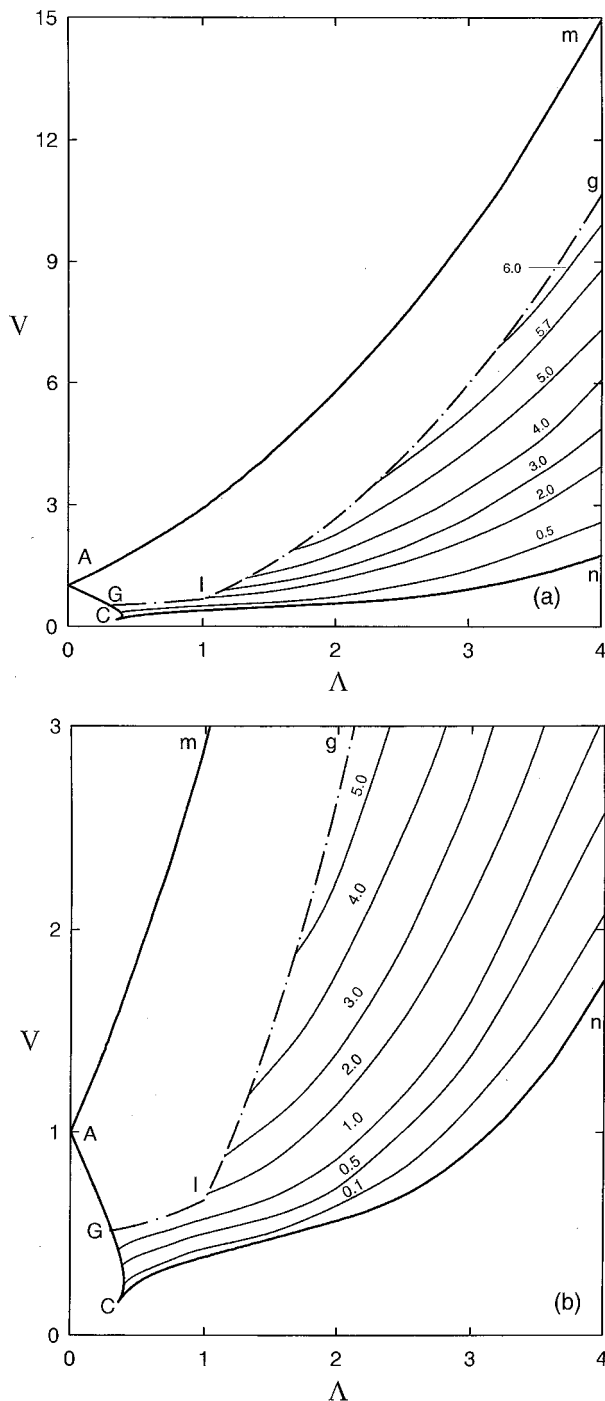


FIG. 22. (a) Lines of constant values of the dimensionless stability margin,  $\Sigma$ , denoted by numbers on curves. (b) Stability margin isolines for  $V \leq 3$ .

particular, for a fixed small and moderate  $\Lambda$  (at least for  $\Lambda \leq 4$ ), the stability margin increases with increasing  $V$  from the minimum volume stability limit up to value of  $V$  at the upper boundary of the strip. This increase in the liquid volume is stabilizing. The larger liquid volume, the larger the magnitude of the perturbations needed to break the liquid bridge. However, the growth rate of the stability margin for a given  $\Lambda$  slows as the maximum volume of the strip is approached. This decrease in  $|dM/dV|$  becomes more evident at larger  $\Lambda$ . In contrast, for long bridges ( $\Lambda \geq 6$ ), the value of

the stability margin initially increases with volume, reaches its maximum within the strip, and then decreases. The decrease of the stability margin is probably due to the rotund nature of the associated axisymmetric bridges. For rotund bridges, the protruding part of a bridge may be torn away under finite magnitude perturbations, whereupon the bridge becomes thinner.

If a point of the stability region lies beyond the strip, the stability margin for the corresponding stable bridge cannot be estimated through the depth of the potential well. Here, only equilibrium configurations with self-intersecting profiles coexist along with a stable bridge. Although a transition to such configurations does not essentially change the topology of the potential energy surface, we cannot consider them as physical liquid bridges and use them to estimate the potential energy barrier. For stable bridges that do not belong to the strip, the stability margin must be estimated using another approach. However, only general ideas of approaches that might be used have been developed (see Ref. 4, pp. 262–269) and they are far more complicated than estimation of the potential energy barrier. As far as we are aware, such approaches have not yet been realized.

Thus, the stability of axisymmetric bridges to finite perturbations has been estimated through a detailed examination of the “stability margin.” If the kinetic and potential energies of initial perturbations exceed the stability margin, a considerable change in the equilibrium state (for example, breakage of the bridge) should be expected.

Experimental investigation of the predictions made here would be interesting. Figure 21, for example, shows the dimensionless stability margin as a function of slenderness. An experimental investigation of the stability margin related to this diagram must involve the imposition of specific perturbations compatible with the class of admissible perturbations used in the analysis. These are perturbations of the liquid bridge surface at constant volume and slenderness. This is in contrast to experimental investigation of the stability limits<sup>15</sup> where either the volume is fixed and the slenderness varied until the stability limit is reached, or where the slenderness is fixed and the volume varied. Acoustic,<sup>16,17</sup> or electrostatic,<sup>18</sup> radiation-pressure techniques could be used to impose well-characterized perturbations at fixed slenderness and volume, and thus would allow for a quantitative experimental investigation.

**ACKNOWLEDGMENTS**

The National Aeronautics and Space Administration supported this work through Grant No. NAG3-2160. One of the authors (L.A.S.) thanks Professor Simon Ostrach and the Case School of Engineering for support through the Wilbur J. Austin Distinguished Professorship.

<sup>1</sup>A. D. Myshkis, “On depressions,” *Zh. Vychisl. Mat. Mat. Fiz.* **5**, 537 (1965) (in Russian); English translation: *USSR Comput. Math. Math. Phys.* **5**, 193 (1965).  
<sup>2</sup>A. D. Myshkis, “Wells in topological spaces,” *Matem. Zametki* **33**, 261 (1983) (in Russian); English translation: *Math. Notes of the Academy of Sciences of the USSR* **33**, 131 (1983).  
<sup>3</sup>A. D. Myshkis, “On the concept of stability margin in problems on the mechanics of continuous media,” in *Introduction to the Dynamics of a*

- Body Containing a Liquid Under Zero-Gravity Conditions* (Vychisl. Tsentr Akad. Nauk SSSR, Moscow, 1968), pp. 269–278 (in Russian).
- <sup>4</sup>A. D. Myshkis, V. G. Babskii, N. D. Kopachevskii, L. A. Slobozhanin, and A. D. Tyuptsov, *Low-Gravity Fluid Mechanics* (Springer-Verlag, Berlin, 1987).
- <sup>5</sup>S. A. Cryer and P. H. Steen, “Collapse of the soap film bridge: quasi-static description,” *J. Colloid Interface Sci.* **154**, 276 (1992).
- <sup>6</sup>J. Plateau, *Statique Experimentale et Theoretique des Liquides* (Gauntier-Villars, Paris, 1873).
- <sup>7</sup>R. D. Gillette and D. C. Dyson, “Stability of fluid interfaces of revolution between equal solid circular plates,” *Chem. Eng. J.* **2**, 44 (1971).
- <sup>8</sup>D. H. Michael, “Meniscus stability,” *Annu. Rev. Fluid Mech.* **13**, 189 (1981).
- <sup>9</sup>E. A. Boucher and T. G. J. Jones, “Equilibrium and stability characteristics of zero-gravity fluid bridges constrained between equal solid rods,” *J. Colloid Interface Sci.* **126**, 469 (1988).
- <sup>10</sup>B. J. Lowry and P. H. Steen, “Capillary surfaces: Stability from families of equilibria with application to the liquid bridge,” *Proc. R. Soc. London, Ser. A* **449**, 411 (1995).
- <sup>11</sup>L. A. Slobozhanin, J. I. D. Alexander, and A. H. Resnick, “Bifurcation of the equilibrium states of a weightless liquid bridge,” *Phys. Fluids* **9**, 1893 (1997).
- <sup>12</sup>J. M. Haynes, “Stability of a fluid cylinder,” *J. Colloid Interface Sci.* **32**, 652 (1970).
- <sup>13</sup>R. Finn, *Equilibrium Capillary Surfaces* (Springer-Verlag, New York, 1986).
- <sup>14</sup>M. A. Erle, R. D. Gillette, and D. C. Dyson, “Stability of interfaces of revolution with constant surface tension. The case of catenoid,” *Chem. Eng. J.* **1**, 97 (1970).
- <sup>15</sup>N. A. Bezdenejnykh, J. Meseguer, and J. M. Perales, “An experimental analysis of the instability of nonaxisymmetric liquid bridges in a gravitational field,” *Phys. Fluids* **11**, 3181 (1999).
- <sup>16</sup>M. J. Marr-Lyon, D. B. Thiessen, and P. L. Marston, “Stabilization of a cylindrical capillary bridge far beyond the Rayleigh-Plateau limit using acoustic radiation pressure and active feedback,” *J. Fluid Mech.* **351**, 345 (1997).
- <sup>17</sup>M. J. Marr-Lyon, D. B. Thiessen, and P. L. Marston, “Passive stabilization of capillary bridges in air with acoustic radiation pressure,” *Phys. Rev. Lett.* **86**, 2293 (2001).
- <sup>18</sup>M. J. Marr-Lyon, D. B. Thiessen, F. J. Blonigen, and P. L. Marston, “Stabilization of electrically conducting capillary bridges using feedback control of radial electrostatic stresses and the shapes of extended bridges,” *Phys. Fluids* **12**, 986 (2000).